


Intrinsic differences and realistic perspectives of lithium-sulfur and magnesium-sulfur batteries

Georg Bieker ¹, Verena Küpers ¹, Martin Kolek ¹✉ & Martin Winter^{1,2}✉

Following in the footsteps of lithium-sulfur batteries, magnesium-sulfur batteries offer a high theoretical energy content and are composed of cheap and more environmentally-friendly electrode materials. In comparison to lithium-sulfur, however, current magnesium-sulfur batteries suffer from higher overpotentials at the magnesium anode and the sulfur cathode, lower material utilization and reversibility at the sulfur cathode, and an excessive demand of electrolyte. Here, a side-by-side comparison of the processes at the two metal anodes and at the sulfur cathode in Li⁺- or Mg²⁺-based electrolytes highlights how most of the challenges facing magnesium-sulfur batteries are intrinsically rooted in the nature of the magnesium species, requiring different research directions than lithium-sulfur batteries. An evaluation of the energy content and the corresponding costs on a practical cell stack level illustrates the importance of overcoming these challenges.

Rechargeable metal-S batteries, such as Li-S, Na-S, K-S, Mg-S, Ca-S, and Al-S batteries¹⁻⁴ use a cathode based on sulfur, a much cheaper, more abundant, and more sustainable material than the typically Li-, Co-, Mn-, and Ni-based cathode materials in lithium ion batteries (LIB)⁵⁻⁷. Furthermore, due to the high capacities of sulfur and the metal anodes, the cell systems correlate with high theoretical energy contents. These are highest for Li-S batteries (LSBs) (2654 Wh kg⁻¹ and 2856 Wh L⁻¹) and Mg-S batteries (MSBs) (1684 Wh kg⁻¹ and 3221 Wh L⁻¹)⁸. Although overpotentials and incomplete active material utilization as well as high amounts of electrolyte and other inactive materials reduce the energy content of practical LSBs and MSBs significantly⁹, these two systems hold the potential for similar or even higher energy contents than LIBs. While in case of LSBs, the cost advantage of the S cathode is counterbalanced by combining it with expensive and locally resource-limited Li as anode material (at least 250 \$ kg⁻¹ for Li metal foils¹⁰, 18 ppm in earth crust¹¹, 0.2 g m⁻³ in sea water¹²), MSBs use cheap and globally abundant Mg as anode material (2.5 \$ kg⁻¹ for Mg metal⁵, 2.2% in earth crust¹¹, 1 kg m⁻³ in sea water¹³). MSBs are therefore highly attractive as a potentially more cost effective and, in term of element abundance and material accessibility⁶, more sustainable alternative to LIBs and LSBs.

Different to alkali and Ca metal anodes, a less negative standard reduction potential of the Mg anode (-2.36 V vs. standard hydrogen electrode, SHE) results in an extraordinary high stability against liquid electrolytes. Accordingly, a mainly surface layer-free anode and a high Coulombic reversibility of Mg electrodeposition and -dissolution of up to 99.9% are observed in numerous electrolyte systems, in particular in cyclic voltammetry experiments¹⁴⁻²¹. In case of Li, Na, K, and Ca metal, in contrast, the lower standard electrode potentials of -3.04 V, -2.71 V, -2.92 V, and -2.87 V vs. SHE, respectively, result in a thermodynamic instability with commonly used organic electrolytes. For the most intensively investigated Li metal anode, the continuous corrosion of the anode is slowed down by a protective solid electrolyte interphase (SEI)²²⁻²⁶ and/or by application of solid electrolytes²⁷⁻²⁹. On Na and K anodes, however, the formation of a protective SEI is complicated by the higher solubility of the Na⁺- and K⁺-containing SEI

¹MEET Battery Research Center, Institute of Physical Chemistry, University of Münster, Münster, Germany. ²Helmholtz Institute Münster (HI MS), IEK-12, Forschungszentrum Jülich GmbH, Münster, Germany. ✉email: martin.kolek@uni-muenster.de; m.winter@fz-juelich.de

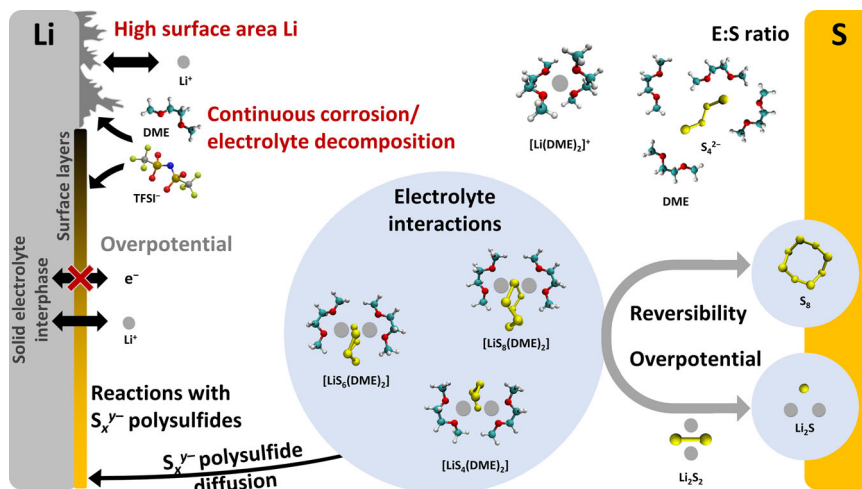


Fig. 1 Summary of the main characteristics and challenges of LSBs. As highlighted in red, research should focus on mitigating the continuous corrosion of the Li metal anode, which is amplified by high-surface-area Li deposits. The molecular structures contain Li (gray), S (yellow), O (red), C (cyan), H (white), and N (blue). Blocked pathways are indicated by red crosses. (Molecular structures are redrawn from Bieker et al.⁸⁴. Copyright American Chemical Society. Reused with permission).

components^{30–32}. On the Ca anode (-2.87 V vs. SHE), in contrast, the formation of electrolyte decomposition surface films results in high overpotentials of Ca electrodeposition and -dissolution or even fully passivates the electrode^{33–35}.

Altogether, combining Mg metal with a sulfur cathode is thus considered a potential breakthrough in the development of low cost and long-lasting metal-S batteries. In state-of-the-art MSBs, however, high overpotentials during Mg electrodeposition and -dissolution at the anode, as well as large amounts of electrolyte, high overpotentials and a low reversibility at the S cathode limit the practically achievable energy content and the corresponding cost advantage. Since many of these challenges vary largely from those of LSBs, also the future directions of MSB research have to deviate from the more widely investigated Li counterpart.

In a side-by-side comparison, this article explains how the different challenges of LSBs and MSBs are rooted in the intrinsically different nature of the involved Li and Mg species. In the first part, the different reactivities of the Li and Mg anode with the commonly used electrolytes, the origins of the higher overpotentials of Mg electrodeposition and -dissolution, as well as the Li and Mg deposit morphologies and safety aspects are discussed. The second part outlines the different stabilization, solubility, and redox behavior of the polysulfide intermediates in Li^+ - and Mg^{2+} -containing electrolytes, and the varying characteristics of Li and Mg sulfides in the composite cathode. In result, it is explained why improving the S cathode performance in MSBs is mostly a question of proper electrolyte design. In a third part, it is presented how the characteristics of the two metal anodes and the sulfur cathode in Li^+ - or Mg^{2+} -based electrolytes are reflected in the overall performance of LSB and MSB cells. An estimation of the energy content and material costs of LSBs and MSBs on a practical cell level, further reveals that MSBs will only be cost competitive to LIBs, if the overpotentials at the Mg and S electrode and the electrolyte-to-sulfur (E:S) ratio can be reduced tremendously. For LSBs, in contrast, it is shown that they might not be cost competitive to LIBs but hold the potential of significantly higher specific energies. In the end, the article provides a perspective on key directions of future MSB research. According to intrinsic differences elaborated within this article, most of these directions deviate substantially from LSB research.

Characteristics of Li and Mg metal anodes. Li and Mg show a diagonal relationship in the periodic table of the elements. Therefore, several chemical characteristics are similar, like the formation of monoxide species during combustion, their reactivity towards nitrogen, and the chemical instability of their carbonates upon heating³⁶. As described in the following, their properties as metal anodes in battery cells, however, differ rather strongly. The resulting challenges of the anode in LSBs and MSBs are summarized in Figs. 1 and 2, respectively.

Stability against the electrolyte. Due to its low standard electrode potential of -3.04 V vs. SHE, Li metal is thermodynamically instable against commonly used liquid organic electrolytes. To slow down continuous corrosion and thus self-discharge of the anode and the degradation of the electrolyte^{26,37,38}, Li metal can be kinetically protected by an electronically insulating, but Li^+ -conductive SEI^{22–26}. To compensate for the volume changes during Li electrodeposition and -dissolution and suppress the formation of high-surface-area lithium (HSAL³⁹, often referred to as heterogeneous or dendritic Li), the SEI further has to be stable, flexible, and homogenous. The formation of a truly long-term protective SEI at the Li metal anode has been investigated for decades^{40–42} and still remains an unsolved challenge for lithium metal-based battery systems, including LSBs^{25,43}. To compensate for the reactivity of the Li metal anode with the electrolyte, LSB cells require an excess of Li metal and high amounts of electrolyte⁹. The latter is usually covered by a high E:S ratio.

At the Mg anode, in contrast, a standard electrode potential of -2.36 V vs. SHE results in a high stability against numerous electrolyte systems. This is expressed by a Coulombic reversibility of Mg electrodeposition and -dissolution of up to 99.9% in cyclic voltammetry experiments^{14–21}. A potential kinetic protection of Mg by surface films is thus considered to play a less relevant role than described above for the Li, Na, K, and Ca anodes. In several electrolyte systems, however, such high Coulombic reversibility is only achieved after a certain number of Mg electrodeposition and -dissolution cycles^{21,44–48}. During this so-called “conditioning” process, the irreversible capacities correspond to the reduction of H_2O or other reducible impurities in the electrolyte^{14,20,49}. In $AlCl_3$ -containing electrolytes, irreversible capacities may also correspond to a corrosion of Mg by $AlCl_2^+$ or other $AlCl_x$

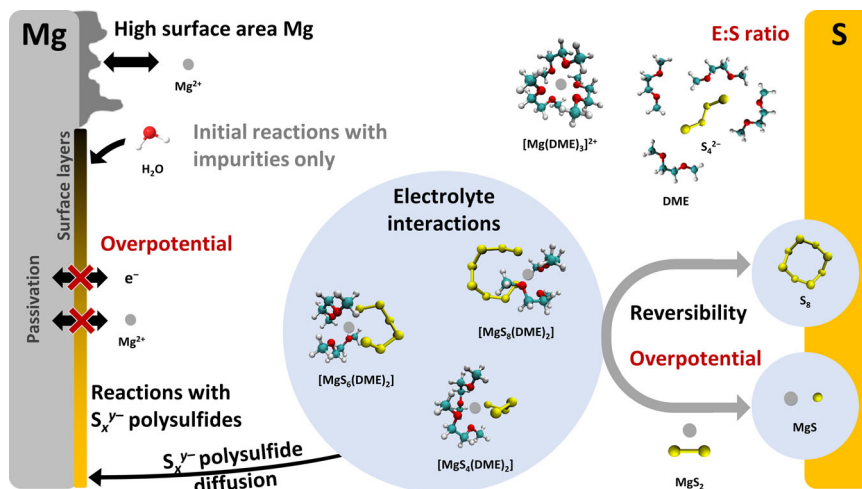


Fig. 2 Summary of the main characteristics and challenges of MSBs. As highlighted in red, research should focus on a reduction of the high overpotentials at the Mg anode and the S cathode, as well as the realization of low E:S ratios. The molecular structures contain Mg (gray), S (yellow), O (red), C (cyan), H (white), and N (blue). Blocked pathways are indicated by red crosses. (Molecular structures are redrawn from Bieker et al.⁸⁴. Copyright American Chemical Society. Reused with permission).

species^{20,44,48,49}. Accordingly, irreversible capacities can be avoided by a pre-treatment of the electrolyte with Mg metal^{48,49} or by directly preparing the electrolyte in an optimized stoichiometry^{20,50} and the addition of reductive species, like Bu_2Mg ^{14,20}.

Overpotentials. Overpotentials during metal electrodeposition and -dissolution mainly result from metal ion conductivity (i) in the electrolyte and (ii) in the surface films, like the SEI in case of Li and potentially fully passivating surface films in case of Mg, and from (iii) energy barriers for ion adsorption and (iv) charge transfer at the electrode|electrolyte interface. Since overpotentials depend on the electrolyte and experimental conditions like current density, a direct comparison of the overpotentials of Li and Mg electrodeposition and -dissolution is difficult. Nevertheless, the hysteresis between the potentials of constant current electrodeposition and -dissolution of Mg (e.g., 0.2–0.3 V in 0.25 M magnesium bis(trifluoromethanesulfonyl)imide (MgTFSI_2)/ MgCl_2 (1:2) in 1,2-dimethoxyethane, DME¹⁴) is usually about one order of magnitude higher than for Li (e.g., below 0.025 V in 1 M lithium bis(trifluoromethanesulfonyl)imide (LiTFSI) in 1,3-dioxolane (DOL):DME electrolyte⁵¹).

The strong difference in electrodeposition and -dissolution behavior of Mg and Li is rooted in the nature of the Li^+ and Mg^{2+} cations. In comparison to Li^+ , the strong electrostatic interactions of the high charge density Mg^{2+} cations are reflected in a lower ionic conductivity of Mg electrolytes (often $< 5 \text{ mS cm}^{-1}$)^{20,21,52–54} than observed for Li electrolytes ($\approx 5–15 \text{ mS cm}^{-1}$)^{51,55}, even though Mg-based electrolytes with weakly coordinating anions show ionic conductivities comparable to Li-based ones (e.g., magnesium tetrakis(hexafluoroisopropoxy) borate ($\text{Mg}[\text{B}(\text{hfp})_4]_2$) with up to 11 mS cm^{-1})^{56,57}. The interactions further inhibit a reasonable mobility of Mg^{2+} in solids⁵⁸. Accordingly, the occurrence of interphase layers, e.g., from the decomposition of electrolyte components or impurities, slows down the electrodeposition and -dissolution of Mg^{2+} and may even passivate the electrode for ion transport^{14,47,59}. The main approach in Mg battery research is thus to maintain a bare and passivation-free Mg anode surface^{60,61}. In addition to choosing electrolyte components that are stable against Mg metal, this may require reductive impurity scavengers, like formerly used Grignard species⁶⁰, small amounts of Bu_2Mg ^{14,20}, or an electrolyte pre-treatment with Mg metal. In

the aforementioned “conditioning” process, reductive currents at potentials above 0 V vs. Mg/Mg^{2+} and a continuous decrease in overpotentials of the Mg electrodeposition and -dissolution indicate an electrochemical “purification”^{14,20,46,47,62}. Here, the decrease in overpotentials is also considered to relate to the formation of Cl^- species, which remove surface layers from the Mg anode and inhibit further adsorption and decomposition of impurities^{14,44,59}.

In addition, a strong coordination of Mg^{2+} with the electrolyte solvent⁶³, which results in high desolvation energies, contributes to the overpotential of Mg electrodeposition¹⁴. Similarly, the insertion of Mg^{2+} into insertion cathode materials is slowed down by the high desolvation energies of Mg^{2+} cations^{64–67}. To lower these overpotentials, the solvent coordination of Mg^{2+} cations needs to be weakened, e.g., by transferring Mg^{2+} into Mg_2Cl_3^+ , $\text{Mg}_2\text{Cl}_2^{2+}$, or other $\text{Mg}_x\text{Cl}_y^{z+}$ complexes^{14,67,68}. As some Cl^- -containing Mg electrolytes are found to be corrosive towards components of the cell housing or the Al current collector, those components might need to be protected by coatings or replaced by corrosion-stable materials^{69,70}.

Deposit morphology. When comparing the deposit morphologies at the Li and Mg metal anode, it is often stated that Li is plagued by HSAL or even dendrite formation^{51,71,72}, while Mg electrodeposition is homogenous and dendrite-free^{60,73}. For the Li metal anode, deposits are found to have a moss-like, needle-like, nodule-like, or granule-like morphology⁵¹. At the Mg anode, deposits are mostly described as pyramidal^{18,74,75} or hexagonal structures^{73,76,77}. This difference is illustrated in a comparative study of Li and Mg electrodeposition and -dissolution at varied current densities by Matsui⁷³.

The different deposit morphologies are mostly explained by a more homogeneous current distribution on a clean, surface film-free Mg electrode^{73,78} in comparison to a heterogeneous current distribution through the multicomponent SEI on Li metal⁷¹. When the SEI breaks upon the volume change of Li electrodeposition and -dissolution, unprotected Li surface is exposed^{25,26,37}. This results in even more heterogeneous current distribution on the electrode surface and thus a self-enforcing mechanism harming performance and safety. By exposing unprotected Li, this mechanism accelerates the corrosion of the electrode. To suppress both, a stable, flexible, and homogeneous SEI is required.

At the Mg anode, the tendency towards more homogenous deposits is further assigned to a low surface diffusion barrier of Mg in comparison to Li metal⁷⁹. Moreover, a local depletion of active Mg species in the electrolyte just after Mg electrodeposition is hypothesized to create a homogenous distribution of Mg nucleation sites⁷³. When comparing to the more heterogeneous deposition of Li, this idea is supported by a usually lower ionic conductivity of Mg electrolytes (often $< 5 \text{ mS cm}^{-1}$)^{20,21,52} in comparison to their Li counterparts ($\approx 5\text{--}15 \text{ mS cm}^{-1}$)^{51,55}, even though a few Mg electrolytes show higher ionic conductivities (e.g., $\text{Mg}[\text{B}(\text{hfp})_4]_2$ with up to 11 mA cm^{-1})⁵⁷. Similarly, the homogenous electrodeposition process is explained by the kinetic barrier of the desolvation of Mg species⁸⁰.

In practice, however, the electrodeposition and -dissolution of Mg is not necessarily homogeneous. In fact, also the formation of high-surface-area magnesium (HSAM) and even Mg dendrites has been reported, especially at higher current densities^{81–83}. Although HSAM seems less reactive with the electrolyte than HSAL, the breaking of HSAM structures may result in electronic contact loss and thus a loss of active materials, as well. Since the structure of Mg deposits depends on the applied current density^{73,76}, the Mg^{2+} complexation in the electrolyte^{74,76,80}, and the presence of surface films on the Mg electrode⁸¹ HSAM formation should be avoided by the electrolyte design and applying suitable current densities.

Safety. In addition to an amplified corrosion of the Li metal anode, the formation of HSAL, in particular in form of Li dendrites, corresponds to the risk of internal short-circuits, when these grow through the separator and reach the cathode. Although the tendency to form dendrites is lower in the case of the Mg metal anode, a high rigidity and hardness of Mg dendrites in comparison to their Li counterparts increase the risk of internal short-circuits also for Mg metal-based batteries⁸².

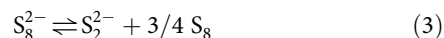
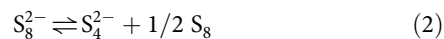
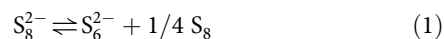
In case of Li metal, also the high reactivity with moisture and air, a low auto-ignition temperature of 180°C and a low melting point of 181°C result in safety concerns. Mg metal, in contrast, has a high auto-ignition temperature of 473°C and a melting point of 650°C . In form of Mg foil, it passivates when in contact with moisture and air at room temperature. Nevertheless, Mg metal is highly inflammable and should therefore be considered a potential safety risk, as well.

Sulfur cathode. At the cathode, the electrolyte needs to be non-nucleophilic and to show a certain oxidative stability in order to be stable towards elemental sulfur. MSBs thus require the deployment of non-nucleophilic and electrochemically stable Mg electrolytes¹⁷. As in LSBs, the overall reduction of elemental sulfur to sulfides during discharge, and the re-oxidation of these species to sulfur during charge proceed through polysulfide intermediates⁸⁴. Nevertheless, MSBs show a different reaction pathway, higher overpotentials and a lower Coulombic reversibility than LSBs. In a side-by-side comparison of the S cathode in Li^+ - or Mg^{2+} -containing electrolytes, the following paragraphs explain how these differences are eventually rooted in the stronger electrostatic interaction of Mg^{2+} with polysulfide and sulfide anions. The challenges of the S cathode in LSBs and MSBs are summarized in Figs. 1 and 2, respectively.

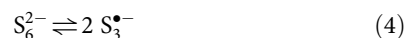
Polysulfides species. Li and Mg polysulfides form a complex system of disproportionation and dissociation equilibria, as depicted in Eqs. 1–4^{84–88}. Here, the disproportionation reaction is considered to be driven by an increased electrostatic interaction of the electrolyte cations with high charge density (often called “short chain”) polysulfides like S_4^{2-} and S_2^{2-} in comparison to

low charge density (often referred to as “long chain”) S_8^{2-} , S_6^{2-} , and $\text{S}_3^{\bullet-}$ species^{84,87}. Accordingly, the stronger Coulomb attraction of Mg^{2+} in comparison to two Li^+ cations, results in a more pronounced disproportionation of polysulfides in Mg electrolytes⁸⁴. At the same time, the dissociation of S_6^{2-} to $\text{S}_3^{\bullet-}$ is observed to be more favored in case of Li^+ coordination^{84,85}.

Disproportionation:



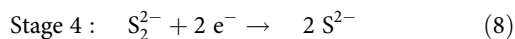
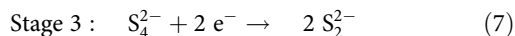
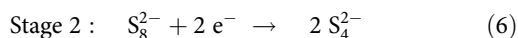
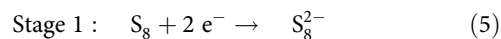
Dissociation:



In ethers like tetrahydrofuran (THF), DME, and tetraethylene glycol dimethyl ether (TEGDME), which are commonly used in LSB and MSB cells, comparably low interactions between the solvent and the cation result in rather strong cation-polysulfide interactions. These favor the disproportionation of low charge density polysulfides to sulfur and high charge density species^{84,85,88}. In ethers, chemically synthesized Li polysulfides with a stoichiometry of Li_2S_8 are observed to disproportionate to S_4^{2-} and $\text{S}_3^{\bullet-}$ species^{84,85,88}, while in the equivalent solutions of Mg polysulfides, these species are observed to disproportionate even further to ultraviolet/visible spectroscopy (UV/Vis) insensitive species like MgS_2 ^{84,85}.

Due to the higher electrostatic interaction of the Mg^{2+} cations with polysulfide anions, also the solubility of Mg polysulfides is substantially lower than for their Li counterparts. In THF, DME, and TEGDME, for instance, the solubility of chemically prepared Mg polysulfide in the stoichiometry of MgS_8 is below 100 mM ^{84,85,89,90}, while Li polysulfides in the stoichiometry of Li_2S_8 can be dissolved to a concentration of 6 M in TEGDME⁹¹.

Cation-dependent reaction pathway. According to the different stabilization of polysulfide species in Li^+ - and Mg^{2+} -containing electrolytes, the discharge reaction at the S cathode varies in LSBs and MSBs. Equations 5–8 summarize all potential stages of this reaction. In ether-based, Li^+ -containing electrolytes, the electrochemical reduction of sulfur proceeds via the formation of both S_4^{2-} (stages 1–2) and S_2^{2-} species (stage 3)^{84,88,92}, while in Mg^{2+} -containing electrolytes, the reduction of sulfur tends to directly proceed to S_2^{2-} intermediates (stages 1–3)^{84,90}.



During constant current discharge of LSB cells, the formation of S_4^{2-} (stage 1–2) and S_2^{2-} species (stage 3), respectively, is indicated by two separate voltage plateaus (Fig. 3a)^{91,93}. In MSB cells, the tendency for a rather direct reduction of sulfur to S_2^{2-} (stage 1–3) is frequently indicated by a single voltage plateau^{56,90,94,95}. In several studies, however, the single voltage plateau is preceded by a slow decrease of the voltage (Fig. 3b)^{89,90} or even two separate voltage plateaus are reported^{96–99}. As in LSBs, these indicate the intermediate formation of S_4^{2-} species (stage 1–2) and their reduction to S_2^{2-} (stage 3). In addition to the fact that different discharge voltage profiles of MSBs are reported for different electrolytes, the pathway of the reduction of sulfur to S_2^{2-} is found to be determined by the solvent-dependent

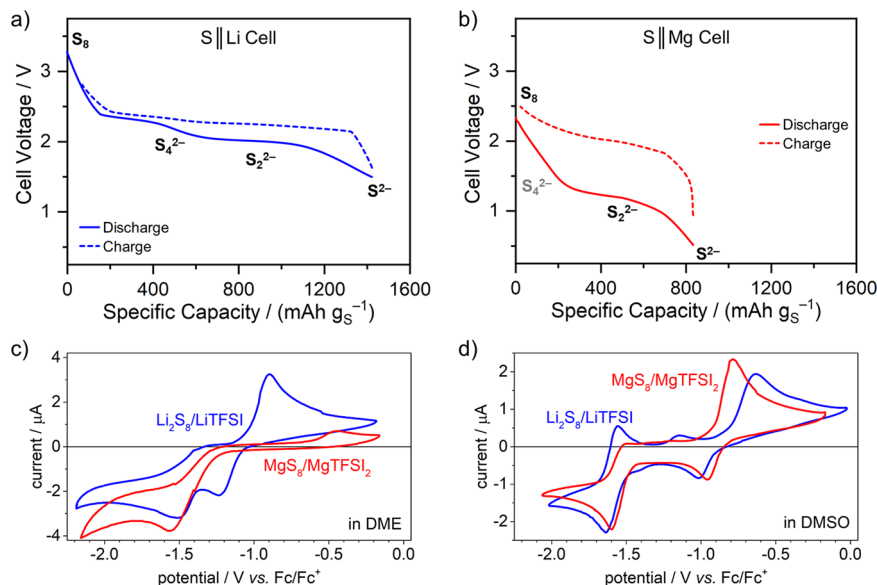


Fig. 3 Cycling profiles of Li-S and Mg-S cells and electrochemical behavior Li and Mg polysulfide solutions. **a/b** Direct comparison of the constant current (100 mA g^{-1}) discharge and charge voltage profiles of a sulfur impregnated activated carbon cloth electrode ($1 \text{ mg}_\text{S} \text{ cm}^{-2}$) in **a** a Li-S cell with 1 M LiTFSI in DME electrolyte during discharge (blue line) and charge (blue dashed line) and **b** a Mg-S cell with 1 M MgTFSI₂/MgCl₂ (1:2) in DME electrolyte during discharge (red line) and charge (red dashed line) (Plots **a** and **b** are reproduced from Gao et al.⁸⁹. Copyright Wiley-VCH Verlag GmbH. Reproduced with permission.)⁸⁹. **c/d** Cyclic voltammograms of a glassy carbon electrode in “Li₂S₈/LiTFSI (1 mM/0.1 M, red line) and “MgS₈/MgTFSI₂ (1 mM/0.05 M, blue line) in **c** DME and **d** DMSO solutions at 50 mV s^{-1} , calibrated vs. (ferrocene | ferrocenium) Fc | Fc⁺ (Figures **c** and **d** are reused from Bieker et al.⁸⁴. Copyright American Chemical Society. Reused with permission).

cation-polysulfide interaction⁸⁴, the composition of the carbon/sulfur (C/S) composite cathode⁹⁰, and the applied discharge rate⁹⁰.

In the final step of the discharge reaction, precipitated S_2^{2-} are reduced to S^{2-} species (stage 4). While this step starts to proceed at a relative constant voltage in LSBs^{91,93}, MSBs show a rather immediate decrease in cell voltage until the lower cut-off voltage is reached^{56,89,90,94–99}.

During charge, LSB cells tend to exhibit two voltage plateaus, corresponding to the formation of polysulfide intermediates and their subsequent oxidation to sulfur^{91,93}. MSB cells, in contrast, mostly show only a single voltage plateau^{90,98,99}. This indicates a lower tendency to form polysulfide intermediates also during charge.

This cation-dependent differences in the electrochemical behavior of the sulfur cathode are also observed in cyclic voltammetry experiments of Li⁺- or Mg²⁺-containing polysulfide solutions⁸⁴. While in solutions of Li₂S₈ and LiTFSI in DME, the reduction of sulfur proceeds via the formation of S_4^{2-} and S_2^{2-} , a direct reduction to S^{2-} is observed in MgS₈/MgTFSI₂ in DME (Fig. 3c).

In order to assess the high voltage of the first step of the discharge reaction and allow a stepwise oxidation during charge, the formation of Mg polysulfide species should be stabilized. Since this stability is determined by the electrostatic interaction of the electrolyte cations with the polysulfide anion, it can be tailored by an effective solvent coordination of the cations. In solvents with high relative dielectric permittivities, like dimethyl sulfoxide (DMSO) or dimethylformamide (DMF), a higher solubility and less disproportionation of Li and Mg polysulfides is observed. Accordingly, the reduction of sulfur in both, Li and Mg, electrolytes proceeds via the formation of low charge density $\text{S}_8^{2-}/\text{S}_6^{2-}$ (stage 1) and high charge density $\text{S}_4^{2-}/\text{S}_2^{2-}$ species (stage 2; Fig. 3d)⁸⁴. Although these particular solvents are considered to passivate the Mg anode, the findings illustrate the beneficial effect of a stronger solvent coordination.

Overpotentials, discharge capacity, and reversibility. LSBs typically show a mean voltage of $\sim 2.1 \text{ V}$ during discharge, while a mean voltage of 2.3 V is observed during charge. Due to the relatively low overpotential of the Li metal anode, this voltage hysteresis almost completely corresponds to overpotentials of the conversion reactions at the sulfur cathode. Accordingly, the potential at the sulfur cathode vs. a Li | Li⁺ reference electrode largely corresponds to the voltage detected in two-electrode Li-S cells¹⁰⁰. With high overpotentials at the Mg anode, in contrast, the voltage in Mg-S cells varies strongly from the potential at the sulfur cathode. When measured vs. a Mg | Mg²⁺ reference electrode, the S cathode shows a mean potential of $1.4\text{--}1.5 \text{ V}$ during discharge and $1.8\text{--}1.9 \text{ V}$ during charge^{89,90}. The charge and discharge reactions of the S cathode in MSBs thus tend to proceed at substantially higher overpotentials than in LSBs.

In both systems, an insufficient electronic contact of sulfur in/to the carbon host structure contributes to overpotentials during discharge^{90,97,99}. In the following, an oversaturation of polysulfide species prior to the nucleation of solid S_2^{2-} and S^{2-} species (stages 2 and 3), which is reported for LSBs^{91,93}, is considered to contribute to the overpotentials in MSB, as well. Since the oversaturation of Li polysulfide species in the liquid phase may reduce the discharge capacity or completely interrupt the discharge process, LSBs require a high amount of electrolyte, usually expressed by the E:S ratio¹⁰¹. Due to the low solubility of Mg polysulfides^{84,85,89,90}, MSBs may reach local oversaturation much faster. This might be the reason why they are usually investigated with E:S ratios of 60:1 or higher^{98,99,102}. In the final step of the discharge reaction, overpotentials are attributed to the slow kinetics of the transformation of amorphous Li₂S₂/MgS₂ to crystalline Li₂S/MgS (stage 4)^{90,96,98}. The overpotentials are amplified by insufficient electronic contact of the sulfide species, which is also rooted in a volume expansion during the transformation of sulfur to Li₂S (181%)⁹³ and MgS (171% in wurtzite and 133% in rock salt structure)⁹⁹, and a poor Li⁺ or Mg²⁺ conductivity of Li₂S and MgS^{90,103}. Although discussed controversially¹⁰⁴, the occurring overpotentials are

considered to impede the full discharge of the S cathode. To maintain a high electronic contact to the sulfur and sulfide species, the active material is embedded into a carbon host structure with a high surface area¹⁰⁵. Similar as for the electrolyte, a high amount of carbon structures favors a high discharge capacity per mass of sulfur⁹⁰. When considering the whole composite cathode, in contrast, the specific capacity will be negatively affected by high amounts of carbon.

During charge, a large activation barrier for re-oxidation of $\text{Li}_2\text{S}/\text{MgS}$ corresponds to large overpotentials and tends to result in an incomplete charge reaction^{90,93,96,98,106,107}. Limiting the discharge process to the formation of MgS_2 thus largely lowers the overpotentials and improves the reversibility of the S cathode⁹⁰. Since the electrostatic interaction of divalent Mg^{2+} with the sulfide anion is higher and the formation of polysulfide intermediates is less favored than in case of monovalent Li^+ cations, overpotentials during charge are more pronounced in the case of MSBs. Accordingly, the addition of Li^+ to an otherwise Mg^{2+} -containing electrolyte lowers the overpotential during charge and improves the overall reversibility of the S cathode¹⁰⁸.

Similarly, it could be shown that in case of the oxidation of chemically prepared Li and Mg polysulfide solutions, a stronger cation-polysulfide interaction in Mg^{2+} -containing electrolytes results in higher overpotentials during their oxidation to sulfur than observed in Li^+ -containing electrolytes (Fig. 3c)⁸⁴. In high dielectric permittivity solvents like DMSO, in contrast, the effective solvent complexation of the Mg^{2+} cation, reduces the cation-polysulfide interaction and lowers the polysulfide oxidation potentials (Fig. 3d)⁸⁴. Since the cation-polysulfide interaction can be weakened by replacing Mg^{2+} by $\text{Mg}_x\text{Cl}_y\text{Z}^z$ species, as well, preliminary results indicate that the oxidation potential of polysulfide species is lowered, if solely MgTFSI_2 -containing electrolytes are substituted by $\text{MgTFSI}_2/\text{MgCl}_2$ -based solutions¹⁰⁹. A suitable complexation of the Mg^{2+} cation by the electrolyte solvent and/or ligands is thus considered a key approach to lower the overpotentials of the sulfur cathode in MSBs.

In an alternative approach, it has been demonstrated that the presence of Cu metal at the S cathode results in lower overpotentials and a higher capacity retention. Thereby, the formation of CuS is observed. During discharge in the presence of Mg^{2+} , CuS is reduced to Cu and MgS, while CuS is formed again during charge¹¹⁰. Over repeated cycling, the reactivity of Cu practically transforms the S cathode into a CuS cathode¹¹¹. Accordingly, these systems are not discussed as MSBs in this article. Moreover, although this system shows lower overpotentials than the conversion of S to MgS, the theoretical specific capacities of such a CuS cathode (561 mAh g^{-1}) is three times lower compared to the S cathode (1672 mAh g^{-1}).

Polysulfide diffusion and reactions with the metal anode. In both, LSBs and MSBs, the S cathode tends to show a substantial capacity fading upon cycling. In addition to a potentially irreversible formation of $\text{Li}_2\text{S}/\text{MgS}$, the capacity fading is related to the diffusion of sulfur and dissolved polysulfide species into the electrolyte. If they reach the metal anode, the reductive decomposition of these species further results in a loss of active material at the anode¹⁰². While still affected, the Li metal anode can be basically protected by the SEI⁹¹. At contrast, the formation of MgS layers on the unprotected Mg anode might result in its passivation¹⁰³. If sulfur or polysulfides with a low charge density (e.g., S_6^{2-} , S_8^{2-}) are only partially reduced to polysulfides with a higher charge density (e.g., S_4^{2-}), these species can diffuse back to the cathode to be re-oxidized. This redox shuttle mechanism corresponds to parasitic currents inside the cell, especially during charging. While being well-known in LSBs^{91,93}, these phenomena also appear in the Mg analogue^{96,98,102,112}. Due to lower

solubility of Mg polysulfides^{84,85,89,90}, this side reaction might be less pronounced in MSBs.

As a main direction of LSB research, countless porous carbon structures and additives are investigated to retard the diffusion of sulfur and dissolved polysulfide species into the electrolyte. Many of these structures are also applied in MSBs. In addition, it has been demonstrated that the diffusion of polysulfides in the electrolyte can be reduced by modified separators^{102,113} and gel polymer electrolytes¹¹⁴. Beyond applying the same materials developed to retain Li polysulfides, however, future MSB research might make use of the high electrostatic attraction of the Mg^{2+} cation to attach it on functional groups of the carbon structures⁹⁸.

For LSBs, at least three alternative approaches are investigated to suppress the dissolution and thus formation of polysulfides: (i) reducing the solubility of polysulfides by the addition of fluorinated co-solvents^{115,116}, by using sparingly solvating electrolytes^{115,117,118}, or by using so-called solvent-in-salt (solvate ionic liquid) electrolytes^{116,119}, (ii) avoiding dissolution of polysulfides either by impregnating sulfur in micropores that are too narrow for solvent molecules^{120–123} or by closing the pores with a semi-permeable cathode electrolyte interphase (CEI)^{120,124,125}, or (iii) avoiding the formation of polysulfide intermediates by using ceramic electrolytes, like sulfide-based glasses^{126,127}. Since all of these approaches increase the overpotentials at the sulfur cathode, they are considered to increase the overpotentials of the S cathode in MSBs even further. Due to the low solubility of Mg polysulfides^{84,85,89,90}, current MSB research might already be similar to the first approach. The second and third approach, however, would be challenged by the low mobility of Mg^{2+} in solids⁵⁸.

Performance, energy content, and cost of practical LSB and MSB cells. In practical LSB and MSB cells, the different characteristics of the two metal anodes and the sulfur cathode in either Li^+ - or Mg^{2+} -based electrolytes are reflected in overall cell performance parameters, such as charge and discharge rate capability, voltage efficiency, and cycle life. Based on what has already been demonstrated in literature, this section provides a direct comparison of several key performance parameters of current LSB and MSB cells. Here, it is illustrated how high overvoltages of current MSB relate to a low voltage efficiency, which would result in high operation costs.

The remainder of the section presents an estimation of the energy content and material cost of LSBs and MSBs on practical cell stack level. Thereby, it is shown that the practically achievable energy content of MSBs is much lower than for LSBs and may not even surpass state-of-the-art LIBs. It is further emphasized that lower overpotentials during charge and discharge and the realization of very low E:S ratios would be required to be more economic than LIBs.

Performance. Figure 4 provides an overview of a selection of cell characteristics and performance parameters usually demonstrated in literature. In this comparison, it is important to note that the first reversible discharge and charge of a sulfur cathode in Mg electrolytes was only demonstrated in 2011¹⁷, while LSB have already been investigated since the 1960s¹²⁸. In Fig. 4, which is largely based on values from a systematic summary of LSB and MSB literature by Chung and Manthiram², this is expressed by a much lower number of publications. A comparison of the current literature thus corresponds to the state-of-the-art in LSB and MSB research but does not necessarily indicate their future potentials.

As discussed in previous sections, the stability of the Mg metal anode with commonly used electrolytes, which is expressed by a

Coulombic reversibility of up to 99.9%^{14–21}, is much higher than usually observed for the Li metal anode. At the same time, although not dendrite-free in all conditions, the deposition morphology of Mg tends to be more homogeneous than observed for Li⁷³. When it comes to overpotentials, however, the Mg metal anode and also the sulfur cathode in Mg electrolytes show significantly higher values than observed for LSBs. On cell level, the hysteresis between a mean discharge voltage of 1.3 V and a mean charge voltage of 2.0 V^{56,89,96,98,99,102}, results in a voltage efficiency of only 65%. For LSBs, the ratio of a mean voltage of 2.1 V during discharge and 2.3 V during charge would achieve a voltage efficiency of up to 91%. When multiplying with Coulombic efficiency, thus including the capacity losses upon charge and discharge, the resulting energy efficiency would correspond to even lower values. During long-term operation, the very low energy efficiency of current MSBs would accumulate to high energy losses, especially when compared to high energy-

efficient LIBs, but also in comparison to LSBs. This would result in higher operating cost¹²⁹.

Figure 4 further indicates how the lower discharge capacity and reversibility of the sulfur cathode in MSBs is reflected in the overall cell performance. First, the sulfur utilization, thus discharge capacity of the cathode when expressed per mass of sulfur, that is reported in current MSBs studies, is usually significantly lower than observed in LSB publications². Second, the capacity of the sulfur cathode is observed to fade significantly faster in MSBs. While in Li⁺-based electrolytes, up to 1000 cycles have been demonstrated in several publications, a reversible operation of the S cathode has, so far, only been demonstrated for ~100 cycles in Mg²⁺-based electrolytes². Moreover, MSB studies only show charge and discharge rates between 0.01 C and 0.1 C, while rates of more than 1 C have already been presented for LSBs². Finally, as already discussed above, the E:S ratio in MSB studies is 60:1 or higher^{98,99,102}, while for LSBs, a stable operation could already be demonstrated with E:S ratios of below 3:1².

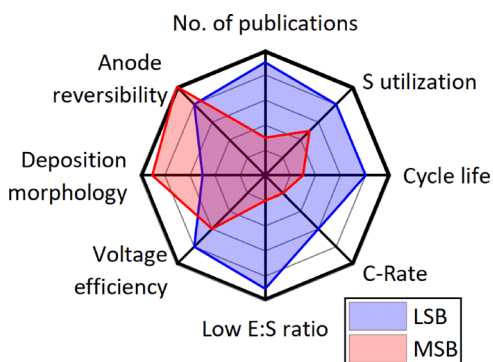


Fig. 4 Cell characteristic and performance parameters of state-of-the-art LSBs and MSBs. Comparison of the number of publications on LSBs (blue) and MSBs (red) and the reported S utilization at the cathode, the cycle life, C-rate, electrolyte-to-sulfur (E:S) ratio, and voltage efficiency on the cell level, as well as the homogeneity of the deposition morphology and electrochemical reversibility at the metal anodes.

Energy content. For the energy content of practical LSB and MSB cells, not only the reversibly realized discharge capacity at the S cathode (as expressed in $\text{mAh g}_\text{S}^{-1}$) and the overall mean discharge voltage, but also the weight and volume of all inactive materials need to be included. Considering that Li, Mg, and S are comparably light-weight active materials, large amounts of electrolyte, the weight of the current collectors and of the carbon host structure have a much stronger impact on the overall specific energy of practical LSB and MSB cells than it is the case in LIBs or solid-state batteries (SSBs), for instance. With an E:S ratio of 3:1, for instance, practical LSB and MSB cells may realize only about 11% of the theoretical specific energy, while in case of practical LIB or SSB cells, 43% and 36%, respectively, of the theoretical specific energy are achieved⁹. Due to the fact that capacity fading and cycle life vary for different cell compositions, the energy content may further change differently during cycling.

Figure 5a–c illustrate how the specific energy of practical LSBs and MSBs is determined by the E:S ratio ($\text{mL g}_\text{S}^{-1}$) and

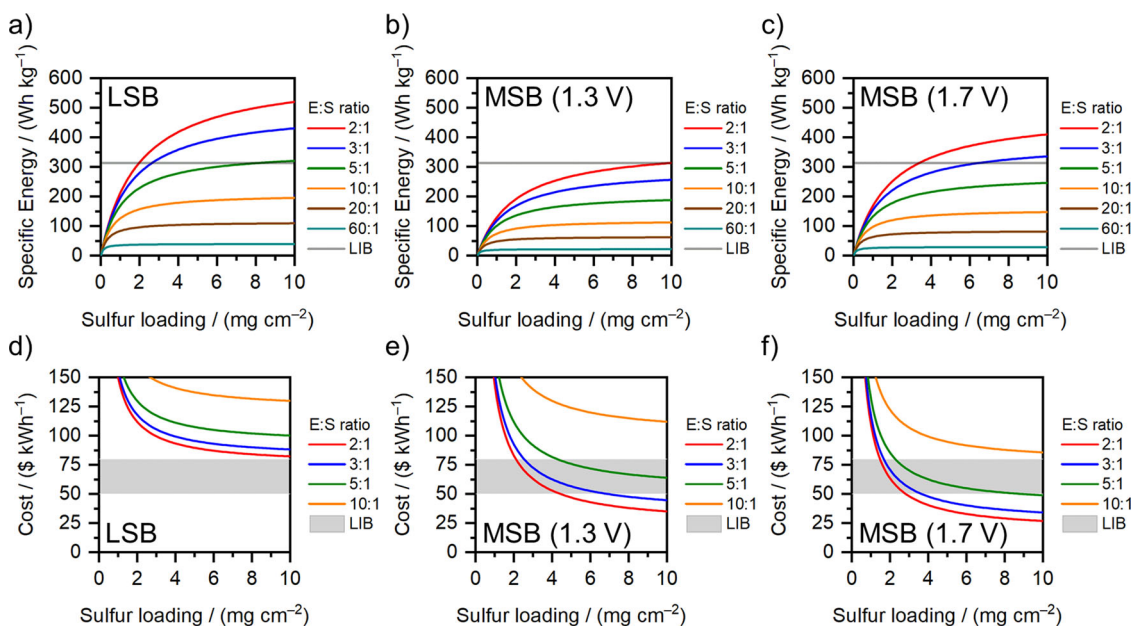


Fig. 5 Specific energy and cost estimations of LSB and MSB. Specific energy on cell stack level (including electrodes, electrolyte, separator, and current collectors) and corresponding material costs in dependence of the electrolyte-to-sulfur (E:S) ratio and sulfur loading for **a/d** LSBs, **b/e** MSBs with the typically observed mean discharge voltage of 1.3 V, and **c/f** MSBs with a hypothetical mean discharge voltage of 1.7 V. E:S ratios of 2:1 (red), 3:1 (blue), 5:1 (green), 10:1 (yellow), 20:1 (brown, only **a-c**), and 60:1 (cyan, only **a-c**) are displayed and compared with state-of-the-art LIBs (gray).

Table 1 Details on the LSB and MSB cells presented in Fig. 5.

Cell	Anode	Cathode	Mean discharge voltage/V	Capacity anode/Ah kg ⁻¹	Excess anode/%	Capacity sulfur/Ah kg ⁻¹	Density electrolyte/kg L ⁻¹
LSB	Li	S/C composite	2.1	3862	100	1200	1
MSB (1.3 V)	Mg	S/C composite	1.3	2205	0	1200	1.1
MSB (1.7 V)	Mg	S/C composite	1.7	2205	0	1200	1.1

Sulfur loading and E:S ratio were varied as displayed in Fig. 5. In all three cell types, the S/C cathode consists of 70 wt.% sulfur, 20 wt.% carbon, and 10 wt.% binder. For the separator, and the Cu (5 μm) and Al current collectors (7.5 μm), a mass of 1.33 mg cm⁻², 4.48 mg cm⁻², and 2.03 mg cm⁻², respectively, has been considered⁹.

the sulfur loading on the electrode (mg cm⁻²). In the case of MSBs, cells with the typically observed mean discharge voltage of 1.3 V^{56,89,96,98,99,102} are compared with cells with a hypothetical mean discharge voltage of 1.7 V, which might be achieved by substantially reducing the overpotentials at the Mg anode and the S cathode. For LSBs, a mean discharge voltage of 2.1 V is used. The displayed values correspond to the cell stack level, so the weight of a pouch, prismatic or cylindrical cell housing is not included. For a comparison with the energy content of state-of-the-art LIBs, the specific energy of a graphite-lithium nickel cobalt aluminum oxide (NCA) cell as estimated by Betz et al.⁹ is indicated. While showing a similar specific energy as expected for graphite-lithium nickel manganese cobalt oxide (NMC811) cells, graphite-NCA cells surpass the energy content of NMC622- or NMC111-based cells¹⁰.

Following the methodology of Betz et al.⁹, a S/C composite with a sulfur content of 70 wt.% and a discharge capacity of 1200 mAh g_S⁻¹ is assumed at the cathode. Here, a typical cathode thickness of 100 μm corresponds to a sulfur loading of 5.8 mg cm⁻². These assumptions are considered optimistic, especially for MSBs. At the Li anode, a Li excess of 100% is considered to compensate for reactions with the electrolyte, while for the less reactive Mg anode no excess is included. All details are displayed in Table 1.

In result, LSBs with E:S ratios of 3:1 and 2:1 provide 394 Wh kg⁻¹ and 467 Wh kg⁻¹, respectively, at a sulfur loading of 5.8 mg cm⁻² (Fig. 5a). When further including the weight of an 18650 cell housing, these values would be reduced to 283 Wh kg⁻¹ and 339 Wh kg⁻¹ in case of LSBs with E:S ratios of 3:1 and 2:1, respectively. Graphite-NCA LIBs correspond to a specific energy of 314 Wh kg⁻¹ on cell stack level and 264 Wh kg⁻¹ on a cell level, based on a set of assumptions⁹. In all, 18650 LSB cells with E:S ratios of 3:1 and 2:1 would significantly surpass the energy content of graphite-NCA cells. Similar values are given in literature^{130,131} and for the LSB prototype cell of Sion Power¹³². Due to the high weight of the 18650 cell housing per cell stack volume, the use of pouch cells would result in LSBs with even higher specific energies. Nevertheless, unlike hard case cell housings, pouch cells do not allow too much excess of liquid electrolyte without losing shape and stability.

MSBs with a typically observed discharge voltage of 1.3 V or lower^{56,89,96,98,99,102} and an E:S ratio of 60:1 or higher^{98,99,102}, correspond to specific energy values of 23 Wh kg⁻¹ or lower. For low E:S ratios of 3:1 and 2:1, however, specific energies of 235 Wh kg⁻¹ and 282 Wh kg⁻¹ would be achieved at a sulfur loading of 5.8 mg cm⁻² (Fig. 5b). In 18650 cells, these values would correspond to an energy content of 178 Wh kg⁻¹ and 217 Wh kg⁻¹¹⁹. Even for such low E:S ratios, MSBs would thus show lower specific energy than graphite-NCA LIBs.

With a hypothetical mean discharge voltage of 1.7 V, in contrast, MSB with E:S ratios of 3:1 and 2:1 could achieve 308 Wh kg⁻¹ and 369 Wh kg⁻¹ on cell stack level (Fig. 5c) and 233 Wh kg⁻¹ and 284 Wh kg⁻¹ in 18650 cells. As for LSBs, the specific energy of such MSBs is considered to be higher in case of pouch cells. Nevertheless, as already indicated on cell stack level, MSBs would

Table 2 Material costs of the LSB and MSB cells presented in Fig. 5d-f.

Material	Cost/\$ kg ⁻¹
Lithium (lower estimate) ¹⁰	250
Lithium (higher estimate) ¹⁰	1000
Magnesium ⁵	5.20
Sulfur ⁵	0.05
Electrolyte ^a	13.64 (15 \$ L ⁻¹)
Copper ^a	13.39 (1.2 \$ m ⁻²)
Aluminum ^a	7.39 (0.3 \$ m ⁻²)
Separator ^a	82.71 (1.1 \$ m ⁻²)
Carbon ¹³³	6.60
Binder ¹³³	9.50

^aCosts in \$ kg⁻¹ were calculated from the values in the BatPaC model¹³³ (in brackets) and the densities or areal mass, respectively, as displayed in Table 1. Note that the Cu and Al current collector foils are considered to be used on both sides.

require largely reduced overpotentials during discharge and very low E:S ratios to achieve similar or even higher specific energy than graphite-NCA LIBs.

Costs. Based on the specific energies of LSBs and MSBs on cell stack level, also the E:S ratio and sulfur loading dependent material costs per kWh are estimated. As displayed in Table 2, the cost of the inactive materials are derived from Argonne National Laboratory's LIB-based BatPaC model¹³³. For Li and Mg electrolytes, the same cost as for a 1.2-M LiPF₆-based electrolyte in BatPaC is assumed (15 \$ L⁻¹), though in particular Mg anodes require specific and highly purified electrolyte solutions. According to the U.S. Geological Survey, a sulfur price of 0.05 \$ kg⁻¹ and a Mg metal price of 5.2 \$ kg⁻¹ are used⁵. In contrast to Mg, the high reactivity with air and moisture, as well as the adhesiveness of Li metal with production equipment is considered to result in higher production costs of Li metal, especially in case of thin foils (e.g., 67 μm for 200% of the capacity of the cathode with a sulfur loading of 5.8 mg cm⁻²). As in a comprehensive cost estimation of LIB and SSB technologies by Schmuck et al.¹⁰, a lower price estimate of 250 \$ kg⁻¹ is compared with a higher estimate of 1000 \$ kg⁻¹ in this study, as well. For Mg, in contrast, it is assumed that the production of thin foils (e.g., 19 μm for 100% of the capacity of the cathode with a sulfur loading of 5.8 mg cm⁻²) will not significantly increase costs.

In Fig. 5d-f, the material price of LSBs and MSBs is compared to the cost range of several currently investigated LIB technologies (on cell stack level). While the higher value of ≈80 \$ kWh⁻¹ corresponds to graphite-NMC622 cells, the lower value of ≈50 \$ kWh⁻¹ is representative for Si/graphite-Li- and Mn-rich NMC cells¹⁰.

For LSBs, the material cost of cell stacks with a sulfur loading of 5.8 mg cm⁻² and E:S ratios of 2:1 to 3:1 is estimated to be 87–93 \$ kWh⁻¹ for the low cost estimate of Li metal (Fig. 5d) and 272–278 \$ kWh⁻¹ for the high cost estimate. While the C/S cathode only contributes 1.30 \$ kWh⁻¹, the Li metal anode

accounts for 62 \$ kWh⁻¹ in the case of a low Li cost of 250 \$ kg⁻¹. For the high cost estimate of 1000 \$ kg⁻¹, the anode alone would correspond to a cost of 247 \$ kWh⁻¹. The electrolyte costs 12–18 \$ kWh⁻¹ for E:S ratios of 2:1 to 3:1 and the other inactive materials would total 13 \$ kWh⁻¹.

In MSBs, in contrast, the low cost of 5.2 \$ kg⁻¹ for Mg metal compensates for the comparatively low specific energy. For cells with the typically observed mean discharge voltage of 1.3 V, very low E:S ratios of 2:1 to 3:1 would result in material costs of 44–53 \$ kWh⁻¹. These are comparable to the lower range of LIBs (Fig. 5e). A significant cost advantage of MSBs over LIBs, however, is only achieved for cells with a discharge voltage higher than 1.7 V, for instance, and very low E:S ratios of 3:1 and 2:1. For a sulfur loading of 5.8 mg cm⁻², such cells would correspond to material costs of 33–41 \$ kWh⁻¹ (Fig. 5f). Here, the S cathode and the Mg anode would contribute with 1.6 \$ kWh⁻¹ and 1.4 \$ kWh⁻¹, respectively, while the electrolyte would cost 15–22 \$ kWh⁻¹ for E:S ratios of 3:1 to 2:1. The separator and current collectors would cost another 16 \$ kWh⁻¹ (at 5.8 mg cm⁻²). In MSBs, electrolyte and other inactive materials are thus the main cost drivers.

In result, the low cost of the Mg and S electrode materials are hardly reflected in the overall material costs per kWh. On the one hand, this is based on a comparably low specific energy on cell stack level of MSBs. On the other hand, the cost advantage over the active materials in LIBs, for instance, diminishes with large amounts of inactive materials in MSBs. When including the cost of further inactive materials, e.g., the cell housing, and the costs of cell production, which may require a pre-treatment and an extremely clean environment in order to avoid the passivation of the Mg metal anode, the cost advantage of the Mg and S electrode materials will diminish further.

Accessible E:S ratio in MSB. Considering that current MSB studies are conducted with E:S ratios of 60:1 or higher^{98,99,102}, which corresponds to a practical energy content of 30 kWh kg⁻¹ or lower (Fig. 5b), the challenge of reducing the amount of electrolyte to a ratio of 3:1 or even 2:1 is tremendous. From a molecular perspective, a ratio of 3 mL DME per gram sulfur, for instance, corresponds to about one solvent molecule per sulfur atom, or 4 solvent molecules per S₄²⁻ species. In other words, 1 g sulfur per 3 mL solvent corresponds to S₄²⁻ or S₈²⁻ concentrations of 2.6 M and 1.3 M, respectively. While for Li₂S₈, a solubility of 6 M is observed in TEGDME⁹¹, for instance, the solubility of MgS₈ is below 100 mM in THF, DME, and TEGDME^{84,85,89,90}. In order to realize MSBs with similar specific energy and lower costs than LIBs, electrolyte formulations with a substantially higher Mg polysulfide solubility need to be developed.

Perspectives on Mg–S batteries. One decade after Kim et al.¹⁷ first reported the reversible charge and discharge of a Mg–S cell, the research on MSBs made tremendous progress. After initial studies with HMDSMgCl/AlCl₃- and MgHMDS₂/MgCl₂/AlCl₃-based electrolytes (HMDS = hexamethyldisilazide)^{17,96–98,102}, the reversible operation of MSBs was also demonstrated in MgCl₂/AlCl₃¹¹², MgTFSI₂/MgCl₂⁸⁹, and Mg[B(OR_F)₄]₂-based electrolytes (R_F = fluorinated alkyl)^{56,57,95}. In parallel, several sulfur/carbon composites already known from LSBs were successfully applied to MSB research^{96,98,102} and the electrochemical processes during charge and discharge at the S cathode in Mg electrolytes have been investigated^{84,90,96,99}.

In a critical perspective, however, this article reveals that it is still a long way to develop state-of-the-art MSB technology into a practical battery technique. First, because of the high voltage hysteresis during charge (2.0 V) and discharge (1.3 V)^{56,89,96,98,99,102}, the voltage efficiency of charging and discharging current MSBs would be below

65%, resulting in an even lower energy efficiency. Second, due to this hysteresis, but also because of high E:S ratios of 60:1 or higher^{98,99,102}, the energy content of current MSBs would be as low as 23 kWh kg⁻¹ on a practical cell stack level. To improve voltage and energy efficiencies and achieve a practical energy content of MSBs to a level comparable to LIBs, future research should focus on the approaches discussed below. A key research direction should be devoted to electrolyte design.

As a first priority, MSB research should focus on lowering the overpotentials at BOTH electrodes. At the Mg anode, the overpotential of electrodeposition and -dissolution can be improved by reducing the strong Mg²⁺ desolvation energies, e.g., by complexing Mg²⁺ with Cl-species. In parallel, the formation of electrode surface films should be avoided by eliminating reducible impurities in the electrolyte by a pre-treatment of the electrolytes, e.g., with Mg metal^{48,49} or reductive species like Bu₂Mg^{14,20}. For a cell behavior free of the need for conditioning, electrolytes should further be prepared in ideal stoichiometry²⁰. At the S cathode, the overpotentials during discharge and charge of the S cathode in Mg electrolytes can be improved by lowering the electrostatic Mg²⁺-polysulfide interaction and stabilizing the formation of Mg polysulfides⁸⁴. Although not stable at the Mg anode, it could be shown in high dielectric permittivity solvents like DMSO and DMF that a higher stabilization of Mg polysulfides increases the mean discharge potential by taking also advantage of the intermediate polysulfide formation⁸⁴. During charge, the intermediate formation of polysulfides lowers the overpotential of oxidation of MgS to sulfur. Similarly, the overpotentials at the S cathode were already found to vary with different ethers^{84,94} and might further be lowered by complexing the Mg²⁺ cation with Cl-species¹⁰⁹.

Second, to achieve practical specific energy values comparable to LIBs, MSB research should focus on realizing tremendously lower E:S ratios. As pointed out in this perspective, the solubility of Mg polysulfides in commonly used ethers is much lower than for Li polysulfides and eventually too low to dissolve sufficiently high amounts of polysulfides in an E:S ratio of 3:1, for instance. Therefore, MSB research should focus on developing electrolytes with a higher Mg polysulfide solubility. At the same time, however, this approach should not promote polysulfide diffusion to the Mg anode to avoid formation of passivating films. Therefore, MSB studies should focus on new ways to anchor or confine dissolved Mg polysulfide species in or at the cathode structure. Differing from LSB research, the high electrostatic interaction of Mg²⁺ with surface groups might open new strategies⁹⁸.

In the end, the technology readiness level (TRL) has to be regarded in the comparison. LIBs are the established high energy density benchmark technology in various markets, while LSBs currently find their way into niche markets and MSBs are in the stage of very basic research. While the specific energy content of practical MSB cells might remain inferior to LIBs and LSBs, it is still too early to state whether or whether not MSBs can be developed into a more economical and more sustainable alternative to these technologies. Differing from LIBs and LSBs, MSBs are rather competitive in terms of electrode material cost, abundant resources, and more ecofriendly active materials^{4,6}. Such systems would be of great interest for a more sustainable integration of renewable energies into the grid.

Received: 2 February 2021; Accepted: 24 February 2021;
Published online: 29 March 2021

References

1. Salama, M. et al. Metal–sulfur batteries: overview and research methods. *ACS Energy Lett.* **4**, 436–446 (2019).

2. Chung, S.-H. & Manthiram, A. Current status and future prospects of metal–sulfur batteries. *Adv. Mater.* **31**, 1901125 (2019).
3. Hong, X. et al. Nonlithium metal–sulfur batteries: steps toward a leap. *Adv. Mater.* **31**, 1802822 (2019).
4. Durmus, Y. E. et al. Side by side battery technologies with lithium-ion based batteries. *Adv. Energy Mater.* **10**, 2000089 (2020).
5. USGS. *Mineral Commodity Summaries 2020* (U.S. Department of the Interior, U.S. Geological Survey, 2020).
6. Dühnen, S. et al. Toward green battery cells: perspective on materials and technologies. *Small Methods* **4**, 2000039 (2020).
7. Winter, M., Barnett, B. & Xu, K. Before li ion batteries. *Chem. Rev.* **118**, 11433–11456 (2018).
8. Zu, C.-X. & Li, H. Thermodynamic analysis on energy densities of batteries. *Energy Environ. Sci.* **4**, 2614–2624 (2011).
9. Betz, J. et al. Theoretical vs. practical energy: a plea for more transparency in the energy calculation of different rechargeable battery systems. *Adv. Energy Mater.* **9**, 1803170 (2018).
10. Schmich, R., Wagner, R., Höppl, G., Placke, T. & Winter, M. Performance and cost of materials for lithium-based rechargeable automotive batteries. *Nat. Energy* **3**, 267–278 (2018).
11. Hans Wedepohl, K. The composition of the continental crust. *Geochim. Cosmochim. Acta* **59**, 1217–1232 (1995).
12. Riley, J. P. & Tongudai, M. The lithium content of sea water. *Deep Sea Res. Oceanogr. Abstr.* **11**, 563–568 (1964).
13. Millero, F. J., Feistel, R., Wright, D. G. & McDougall, T. J. The composition of Standard Seawater and the definition of the Reference-Composition Salinity Scale. *Deep Sea Res. Part I* **55**, 50–72 (2008).
14. Shterenberg, I. et al. Evaluation of (CF₃SO₂)₂N⁻ (TFSI) based electrolyte solutions for Mg batteries. *J. Electrochem. Soc.* **162**, A7118–A7128 (2015).
15. Aurbach, D. et al. Prototype systems for rechargeable magnesium batteries. *Nature* **407**, 724–727 (2000).
16. Aurbach, D. et al. Electrolyte solutions for rechargeable magnesium batteries based on organomagnesium chloroaluminate complexes. *J. Electrochem. Soc.* **149**, A115–A121 (2002).
17. Kim, H. S. et al. Structure and compatibility of a magnesium electrolyte with a sulphur cathode. *Nat. Commun.* **2**, 427 (2011).
18. Doe, R. E. et al. Novel, electrolyte solutions comprising fully inorganic salts with high anodic stability for rechargeable magnesium batteries. *Chem. Commun.* **50**, 243–245 (2014).
19. Liao, C. et al. The unexpected discovery of the Mg(HMDS)₂/MgCl₂ complex as a magnesium electrolyte for rechargeable magnesium batteries. *J. Mater. Chem. A* **3**, 6082–6087 (2015).
20. Bieker, G. et al. The power of stoichiometry: conditioning and speciation of MgCl₂/AlCl₃ in tetraethylene glycol dimethyl ether-based electrolytes. *ACS Appl. Mater. Interfaces* **11**, 24057–24066 (2019).
21. Zhao-Karger, Z., Zhao, X., Fuhr, O. & Fichtner, M. Bisamide based non-nucleophilic electrolytes for rechargeable magnesium batteries. *RSC Adv.* **3**, 16330–16335 (2013).
22. Peled, E. The electrochemical behavior of alkali and alkaline earth metals in nonaqueous battery systems—the solid electrolyte interphase model. *J. Electrochem. Soc.* **126**, 2047–2051 (1979).
23. Peled, E., Golodnitsky, D. & Ardel, G. Advanced model for solid electrolyte interphase electrodes in liquid and polymer electrolytes. *J. Electrochem. Soc.* **144**, L208–L210 (1997).
24. Aurbach, D., Zinigrad, E., Cohen, Y. & Teller, H. A short review of failure mechanisms of lithium metal and lithiated graphite anodes in liquid electrolyte solutions. *Solid State Ionics* **148**, 405–416 (2002).
25. Winter, M. The solid electrolyte interphase – the most important and the least understood solid electrolyte in rechargeable Li batteries. *Z. Phys. Chem.* **223**, 1395–1406 (2009).
26. Bieker, G., Winter, M. & Bieker, P. Electrochemical in situ investigations of SEI and dendrite formation on the lithium metal anode. *Phys. Chem. Chem. Phys.* **17**, 8670–8679 (2015).
27. Placke, T., Kloepsch, R., Dühnen, S. & Winter, M. Lithium ion, lithium metal, and alternative rechargeable battery technologies: the odyssey for high energy density. *J. Solid State Electrochem* **21**, 1939–1964 (2017).
28. Janek, J. & Zeier, W. G. A solid future for battery development. *Nat. Energy* **1**, 16141 (2016).
29. Li, M. et al. Solid-state lithium–sulfur battery enabled by thio-LiSICON/polymer composite electrolyte and sulfurized polyacrylonitrile cathode. *Adv. Funct. Mater.* **30**, 1910123 (2020).
30. Seh, Z. W., Sun, J., Sun, Y. & Cui, Y. A highly reversible room-temperature sodium metal anode. *ACS Cent. Sci.* **1**, 449–455 (2015).
31. Wei, S. et al. A stable room-temperature sodium-sulfur battery. *Nat. Commun.* **7**, 11722 (2016).
32. Wang, L., Bao, J., Liu, Q. & Sun, C.-F. Concentrated electrolytes unlock the full energy potential of potassium-sulfur battery chemistry. *Energy Storage Mater.* **18**, 470–475 (2019).
33. Li, Z., Fuhr, O., Fichtner, M. & Zhao-Karger, Z. Towards stable and efficient electrolytes for room-temperature rechargeable calcium batteries. *Energy Environ. Sci.* **12**, 3496–3501 (2019).
34. Wang, D. et al. Plating and stripping calcium in an organic electrolyte. *Nat. Mater.* **17**, 16–20 (2017).
35. Shyamsunder, A., Blanc, L. E., Assoud, A. & Nazar, L. F. Reversible calcium plating and stripping at room temperature using a borate salt. *ACS Energy Lett* **4**, 2271–2276 (2019).
36. Holleman, A. F., Wiberg, N. & Wiberg, E. *Lehrbuch der Anorganischen Chemie* (De Gruyter, 2007).
37. Kolesnikov, A. et al. Galvanic corrosion of lithium-powder-based electrodes. *Adv. Energy Mater.* **10**, 2000017 (2020).
38. Lin, D. et al. Fast galvanic lithium corrosion involving a Kirkendall-type mechanism. *Nat. Chem.* **11**, 382–389 (2019).
39. Becking, J. et al. Lithium-metal foil surface modification: an effective method to improve the cycling performance of lithium-metal batteries. *Adv. Mater. Interfaces* **4**, 1700166 (2017).
40. Stan, M. C. et al. Sputter coating of lithium metal electrodes with lithiophilic metals for homogeneous and reversible lithium electrodeposition and electrodisolution. *Mater. Today* **39**, 137–145 (2020).
41. Wang, H., Liu, Y., Li, Y. & Cui, Y. Lithium metal anode materials design: interphase and host. *Electrochem. Energy Rev.* **2**, 509–517 (2019).
42. Cheng, X.-B. et al. A review of solid electrolyte interphases on lithium metal anode. *Adv. Sci.* **3**, 1500213 (2016).
43. Shen, X. et al. The failure of solid electrolyte interphase on Li metal anode: structural uniformity or mechanical strength? *Adv. Energy Mater.* **10**, 1903645 (2020).
44. See, K. A. et al. The interplay of Al and Mg speciation in advanced Mg battery electrolyte solutions. *J. Am. Chem. Soc.* **138**, 328–337 (2016).
45. See, K. A., Liu, Y.-M., Ha, Y., Barile, C. J. & Gewirth, A. A. Effect of concentration on the electrochemistry and speciation of the magnesium aluminum chloride complex electrolyte solution. *ACS Appl. Mater. Interfaces* **9**, 35729–35739 (2017).
46. Barile, C. J., Barile, E. C., Zavadil, K. R., Nuzzo, R. G. & Gewirth, A. A. Electrolytic conditioning of a magnesium aluminum chloride complex for reversible magnesium deposition. *J. Phys. Chem. C* **118**, 27623–27630 (2014).
47. Barile, C. J., Nuzzo, R. G. & Gewirth, A. A. Exploring salt and solvent effects in chloride-based electrolytes for magnesium electrodeposition and dissolution. *J. Phys. Chem. C* **119**, 13524–13534 (2015).
48. Merrill, L. C. & Schaefer, J. L. Electrochemical properties and speciation in Mg(HMDS)₂-based electrolytes for magnesium batteries as a function of ethereal solvent type and temperature. *Langmuir* **33**, 9426–9433 (2017).
49. Luo, J., He, S. & Liu, T. L. Tertiary Mg/MgCl₂/AlCl₃ inorganic Mg²⁺ electrolytes with unprecedented electrochemical performance for reversible Mg deposition. *ACS Energy Lett.* **2**, 1197–1202 (2017).
50. Zhao-Karger, Z. et al. Novel transmetalation reaction for electrolyte synthesis for rechargeable magnesium batteries. *RSC Adv.* **4**, 26924–26927 (2014).
51. Küpers, V., Kolek, M., Bieker, P., Winter, M. & Bruncklaus, G. In situ ⁷Li-NMR analysis of lithium metal surface deposits with varying electrolyte compositions and concentrations. *Phys. Chem. Chem. Phys.* **21**, 26084–26094 (2019).
52. Cheng, Y. et al. Highly active electrolytes for rechargeable Mg batteries based on a [Mg₂(μ-Cl)₂]²⁺ cation complex in dimethoxyethane. *Phys. Chem. Chem. Phys.* **17**, 13307–13314 (2015).
53. Küpers, V. et al. Approaching electrochemical limits of Mg₂Cl₇^{z+} complex-based electrolytes for Mg batteries by tailoring the solution structure. *J. Electrochem. Soc.* **167**, 160505 (2020).
54. Ha, S.-Y. et al. Magnesium(II) bis(trifluoromethane sulfonyl) imide-based electrolytes with wide electrochemical windows for rechargeable magnesium batteries. *ACS Appl. Mater. Interfaces* **6**, 4063–4073 (2014).
55. Xu, K. Nonaqueous liquid electrolytes for lithium-based rechargeable batteries. *Chem. Rev.* **104**, 4303–4418 (2004).
56. Zhao-Karger, Z., Gil Bardaji, M. E., Fuhr, O. & Fichtner, M. A new class of non-corrosive, highly efficient electrolytes for rechargeable magnesium batteries. *J. Mater. Chem. A* **5**, 10815–10820 (2017).
57. Zhao-Karger, Z. et al. Toward highly reversible magnesium–sulfur batteries with efficient and practical Mg[B(hfip)₄]₂ electrolyte. *ACS Energy Lett.* **3**, 2005–2013 (2018).
58. Levi, E., Levi, M. D., Chasid, O. & Aurbach, D. A review on the problems of the solid state ions diffusion in cathodes for rechargeable Mg batteries. *J. Electroceram.* **22**, 13–19 (2009).
59. Connell, J. G. et al. Tuning the reversibility of Mg anodes via controlled surface passivation by H₂O/Cl⁻ in organic electrolytes. *Chem. Mater.* **28**, 8268–8277 (2016).
60. Attias, R., Salama, M., Hirsch, B., Goffer, Y. & Aurbach, D. Anode-electrolyte interfaces in secondary magnesium. *Batteries. Joule* **3**, 27–52 (2019).

61. Besenhard, J. O. & Winter, M. Advances in battery technology: rechargeable magnesium batteries and novel negative-electrode materials for lithium ion batteries. *ChemPhysChem* **3**, 155–159 (2002).
62. Shterenberg, I., Salama, M., Gofar, Y., Levi, E. & Aurbach, D. The challenge of developing rechargeable magnesium batteries. *MRS Bull.* **39**, 453–460 (2014).
63. Salama, M. et al. Unique behavior of dimethoxyethane (DME)/Mg(N(SO₂CF₃)₂)₂ solutions. *J. Phys. Chem. C* **120**, 19586–19594 (2016).
64. Wan, L. F., Perdue, B. R., Applett, C. A. & Prendergast, D. Mg desolvation and intercalation mechanism at the Mo₆S₈ chevrel phase surface. *Chem. Mater.* **27**, 5932–5940 (2015).
65. Nam, K. W. et al. The high performance of crystal water containing manganese birnessite cathodes for magnesium batteries. *Nano Lett* **15**, 4071–4079 (2015).
66. Sun, X., Duffort, V., Mehdi, B. L., Browning, N. D. & Nazar, L. F. Investigation of the mechanism of Mg insertion in birnessite in nonaqueous and aqueous rechargeable Mg-Ion batteries. *Chem. Mater.* **28**, 534–542 (2016).
67. Attias, R. et al. The role of surface adsorbed Cl⁻ complexes in rechargeable magnesium batteries. *ACS Catal.* **10**, 7773–7784 (2020).
68. Salama, M. et al. Structural analysis of magnesium chloride complexes in dimethoxyethane solutions in the context of Mg batteries research. *J. Phys. Chem. C* **121**, 24909–24918 (2017).
69. Wall, C., Zhao-Karger, Z. & Fichtner, M. Corrosion resistance of current collector materials in bisamide based electrolyte for magnesium batteries. *ECS Electrochem. Lett.* **4**, C8–C10 (2015).
70. Yagi, S., Tanaka, A., Ichikawa, Y., Ichitsubo, T. & Matsubara, E. Electrochemical stability of magnesium battery current collectors in a grignard reagent-based electrolyte. *J. Electrochem. Soc.* **160**, C83–C88 (2013).
71. Lin, D., Liu, Y. & Cui, Y. Reviving the lithium metal anode for high-energy batteries. *Nat. Nanotechnol.* **12**, 194–206 (2017).
72. Guan, X. et al. Controlling nucleation in lithium metal anodes. *Small* **14**, 1801423 (2018).
73. Matsui, M. Study on electrochemically deposited Mg metal. *J. Power Sources* **196**, 7048–7055 (2011).
74. Aurbach, D., Cohen, Y. & Moshkovich, M. The study of reversible magnesium deposition by in situ scanning tunneling microscopy. *Electrochem. Solid State Lett.* **4**, A113–A116 (2001).
75. Aurbach, D., Moshkovich, M., Schechter, A. & Turgeman, R. Magnesium deposition and dissolution processes in ethereal grignard salt solutions using simultaneous EQCM-EIS and in situ FTIR spectroscopy. *Electrochem. Solid State Lett.* **3**, 31–34 (2000).
76. Yoo, H. D. et al. Mg rechargeable batteries: an on-going challenge. *Energy Environ. Sci.* **6**, 2265–2279 (2013).
77. Gregory, T. D., Hoffman, R. J. & Winterton, R. C. Nonaqueous electrochemistry of magnesium applications to energy storage. *J. Electrochem. Soc.* **137**, 775–780 (1990).
78. Kim, D. Y., Lim, Y., Roy, B., Ryu, Y.-G. & Lee, S.-S. Operating mechanisms of electrolytes in magnesium ion batteries: chemical equilibrium, magnesium deposition, and electrolyte oxidation. *Phys. Chem. Chem. Phys.* **16**, 25789–25798 (2014).
79. Jäckle, M., Helmbrecht, K., Smits, M., Stottmeister, D. & Groß, A. Self-diffusion barriers: possible descriptors for dendrite growth in batteries? *Energy Environ. Sci.* **11**, 3400–3407 (2018).
80. Hu, X.-C. et al. Direct insights into the electrochemical processes at anode/electrolyte interfaces in magnesium-sulfur batteries. *Nano Energy* **49**, 453–459 (2018).
81. Ding, M. S., Diemant, T., Behm, R. J., Passerini, S. & Giffin, G. A. Dendrite growth in Mg metal cells containing Mg(TFSI)₂/glyme electrolytes. *J. Electrochem. Soc.* **165**, A1983–A1990 (2018).
82. Davidson, R. et al. Formation of magnesium dendrites during electrodeposition. *ACS Energy Lett.* **4**, 375–376 (2019).
83. Song, Z. et al. Insights into interfacial speciation and deposition morphology evolution at Mg-electrolyte interfaces under practical conditions. *J. Energy Chem.* **48**, 299–307 (2020).
84. Bieker, G. et al. The cation-dependent electrochemistry of polysulfides in lithium and magnesium electrolyte solutions. *J. Phys. Chem. C* **122**, 21770–21783 (2018).
85. Bieker, G. et al. Influence of cations in lithium and magnesium polysulfide solutions: dependence of the solvent chemistry. *Phys. Chem. Chem. Phys.* **19**, 11152–11162 (2017).
86. Vijayakumar, M. et al. Molecular structure and stability of dissolved lithium polysulfide species. *Phys. Chem. Chem. Phys.* **16**, 10923–10932 (2014).
87. Assary, R. S., Curtiss, L. A. & Moore, J. S. Toward a molecular understanding of energetics in Li-S batteries using nonaqueous electrolytes: a high-level quantum chemical study. *J. Phys. Chem. C* **118**, 11545–11558 (2014).
88. Zou, Q. & Lu, Y.-C. Solvent-dictated lithium sulfur redox reactions: an operando UV-vis spectroscopic study. *J. Phys. Chem. Lett.* **7**, 1518–1525 (2016).
89. Gao, T. et al. Reversible S₀/MgS_x redox chemistry in MgTFSI₂-MgCl₂ electrolyte for rechargeable Mg/S battery. *Angew. Chem.* **129**, 13711–13715 (2017).
90. Gao, T. et al. Thermodynamics and kinetics of sulfur cathode during discharge in MgTFSI₂-DME electrolyte. *Adv. Mater.* **30**, 1704313 (2018).
91. Zhang, S., Ueno, K., Dokko, K. & Watanabe, M. Recent advances in electrolytes for lithium-sulfur batteries. *Adv. Energy Mater.* **5**, 1500117 (2015).
92. Lu, Y.-C., He, Q. & Gasteiger, H. A. Probing the lithium-sulfur redox reactions: a rotating-ring disk electrode study. *J. Phys. Chem. C* **118**, 5733–5741 (2014).
93. Nazar, L. F., Cuisinier, M. & Pang, Q. Lithium-sulfur batteries. *MRS Bull.* **39**, 436–442 (2014).
94. Bevilacqua, S. C., Pham, K. H. & See, K. A. Effect of the electrolyte solvent on redox processes in Mg-S batteries. *Inorg. Chem.* **58**, 10472–10482 (2019).
95. Zhang, Z. et al. Novel design concepts of efficient Mg-Ion Electrolytes toward high-performance magnesium-selenium and magnesium-sulfur batteries. *Adv. Energy Mater.* **7**, 1602055 (2017).
96. Zhao-Karger, Z. et al. Performance improvement of magnesium sulfur batteries with modified non-nucleophilic electrolytes. *Adv. Energy Mater.* **5**, 1401155 (2015).
97. Sievert, B., Häcker, J., Bienen, F., Wagner, N. & Friedrich, K. A. Magnesium sulfur battery with a new magnesium powder anode. *ECS Trans.* **77**, 413–424 (2017).
98. Vinayan, B. P. et al. Performance study of magnesium-sulfur battery using a graphene based sulfur composite cathode electrode and a non-nucleophilic Mg electrolyte. *Nanoscale* **8**, 3296–3306 (2016).
99. Robba, A. et al. Mechanistic study of magnesium-sulfur batteries. *Chem. Mater.* **29**, 9555–9564 (2017).
100. Gröbmeyer, A., Becking, J., Bieker, P. M., Winter, M. & Stan, M. C. A facile preparation of S₀/C composite cathode for lithium-sulfur cells: influence of intrinsic and extrinsic cathode properties on the electrochemical performance. *Energy Technol.* **7**, 1800789 (2019).
101. Hagen, M., Fanz, P. & Tübke, J. Cell energy density and electrolyte/sulfur ratio in Li-S cells. *J. Power Sources* **264**, 30–34 (2014).
102. Yu, X. & Manthiram, A. Performance enhancement and mechanistic studies of magnesium-sulfur cells with an advanced cathode structure. *ACS Energy Lett.* **1**, 431–437 (2016).
103. Salama, M. et al. On the feasibility of practical Mg-S batteries: practical limitations associated with metallic magnesium anodes. *ACS Appl. Mater. Interfaces* **10**, 36910–36917 (2018).
104. Drvarić Talian, S. et al. Which process limits the operation of a Li-S system? *Chem. Mater.* **31**, 9012–9023 (2019).
105. Manthiram, A., Fu, Y., Chung, S.-H., Zu, C. & Su, Y.-S. Rechargeable lithium-sulfur batteries. *Chem. Rev.* **114**, 11751–11787 (2014).
106. Waluś, S. et al. Non-woven carbon paper as current collector for Li-ion/Li₂S system: understanding of the first charge mechanism. *Electrochim. Acta* **180**, 178–186 (2015).
107. Xu, Y. et al. In situ X-ray absorption spectroscopic investigation of the capacity degradation mechanism in Mg/S batteries. *Nano Lett.* **19**, 2928–2934 (2019).
108. Gao, T. et al. Enhancing the reversibility of Mg/S battery chemistry through Li⁺ mediation. *J. Am. Chem. Soc.* **137**, 12388–12393 (2015).
109. Bieker, G. *Reaction Mechanisms in Magnesium/Sulfur Batteries – Chemical and Electrochemical Processes in the Electrolyte, at the Magnesium Metal Anode and at the Sulfur Cathode* (University of Münster, 2019).
110. He, P., Ford, H. O., Merrill, L. C. & Schaefer, J. L. Investigation of the effects of copper nanoparticles on magnesium-sulfur battery performance: how practical is metallic copper addition? *ACS Appl. Energy Mater.* **2**, 6800–6807 (2019).
111. Robba, A. et al. Role of Cu current collector on electrochemical mechanism of Mg-S battery. *J. Power Sources* **450**, 227672 (2020).
112. Li, W. et al. Synthesis, crystal structure, and electrochemical properties of a simple magnesium electrolyte for magnesium/sulfur batteries. *Angew. Chem.* **128**, 6516–6520 (2016).
113. Hunter, O. F., Laura, C. M., Peng, H., Sunil, P. U. & Jennifer, S. Crosslinked ionomer gel separators for polysulfide shuttle mitigation in magnesium-sulfur batteries: elucidation of structure-property relationships. *Macromolecules* **51**, 8629–8636 (2018).
114. Qu, H. et al. Multifunctional sandwich-structured electrolyte for high-performance lithium-sulfur batteries. *Adv. Sci.* **5**, 1700503 (2018).
115. Cheng, L. et al. Sparingly solvating electrolytes for high energy density lithium-sulfur batteries. *ACS Energy Lett.* **1**, 503–509 (2016).
116. Dokko, K. et al. Solvate ionic liquid electrolyte for Li-S batteries. *J. Electrochem. Soc.* **160**, A1304–A1310 (2013).
117. Cuisinier, M. et al. Unique behaviour of nonsolvents for polysulfides in lithium-sulphur batteries. *Energy Environ. Sci.* **7**, 2697–2705 (2014).
118. Shyamsunder, A. et al. Inhibiting polysulfide shuttle in lithium-sulfur batteries through low-ion-pairing salts and a triflamide solvent. *Angew. Chem. Int. Ed.* **56**, 6192–6197 (2017).

119. Suo, L., Hu, Y.-S., Li, H., Armand, M. & Chen, L. A new class of Solvent-in-Salt electrolyte for high-energy rechargeable metallic lithium batteries. *Nat. Commun.* **4**, 1481 (2013).
120. Markevich, E., Salitra, G., Talyosef, Y., Chesneau, F. & Aurbach, D. Review—on the mechanism of quasi-solid-state lithiation of sulfur encapsulated in microporous carbons: is the existence of small sulfur molecules necessary? *J. Electrochem. Soc.* **164**, A6244–A6253 (2017).
121. Wang, D.-W. et al. A microporous-mesoporous carbon with graphitic structure for a high-rate stable sulfur cathode in carbonate solvent-based Li-S batteries. *Phys. Chem. Chem. Phys.* **14**, 8703–8710 (2012).
122. Xin, S. et al. Smaller sulfur molecules promise better lithium–sulfur batteries. *J. Am. Chem. Soc.* **134**, 18510–18513 (2012).
123. Helen, M. et al. Single step transformation of sulphur to $\text{Li}_2\text{S}_2/\text{Li}_2\text{S}$ in Li-S batteries. *Sci. Rep.* **5**, 12146 (2015).
124. Rosenman, A. et al. Facile synthesis and very stable cycling of polyvinylidene dichloride derived carbon: sulfur composite cathode. *J. Electrochem. Soc.* **163**, A1829–A1835 (2016).
125. Markevich, E. et al. The effect of a solid electrolyte interphase on the mechanism of operation of lithium–sulfur batteries. *J. Mater. Chem. A* **3**, 19873–19883 (2015).
126. Yamada, T. et al. All solid-state lithium–sulfur battery using a glass-type $\text{P}_2\text{S}_5\text{-Li}_2\text{S}$ electrolyte: benefits on anode kinetics. *J. Electrochem. Soc.* **162**, A646–A651 (2015).
127. Han, F. et al. High-performance all-solid-state lithium–sulfur battery enabled by a mixed-conductive Li_2S nanocomposite. *Nano Lett.* **16**, 4521–4527 (2016).
128. Ji, X. & Nazar, L. F. Advances in Li-S batteries. *J. Mater. Chem.* **20**, 9821–9826 (2010).
129. Meister, P. et al. Best practice: performance and cost evaluation of lithium ion battery active materials with special emphasis on energy efficiency. *Chem. Mater.* **28**, 7203–7217 (2016).
130. Hagen, M. et al. Lithium–sulfur cells: the gap between the state-of-the-art and the requirements for high energy battery cells. *Adv. Energy Mater.* **5**, 1401986 (2015).
131. Dörfler, S. et al. Challenges and key parameters of lithium–sulfur batteries on pouch cell level. *Joule* **4**, 539–554 (2020).
132. Mikhaylik, Y. V. et al. High energy rechargeable Li-S cells for EV application: status, remaining problems and solutions. *ECS Trans.* **25**, 23–34 (2009).
133. Nelson, P. A. et al. *BatPaC (Battery Performance and Cost) Software 4.0* (Argonne National Laboratory, 2020).

Acknowledgements

The authors wish to thank the German Federal Ministry of Education and Research (BMBF) and the Israeli Ministry of Science and Technology (MOST) for funding this work through the joint project “MgMeAnS” (03XP0140) and the Heinrich Böll

Foundation for funding this work through a PhD scholarship. Moreover, the funding within the BMBF project “MEET Hi-EnD III” (03XP0258A) is acknowledged.

Author contributions

G.B. and M.W. initiated this manuscript. G.B., supported by V.K. and M.K., wrote the manuscript with contributions from M.W. G.B. conducted specific energy and cost estimations. All authors discussed and revised the manuscript and have given approval to its final version.

Funding

Open Access funding enabled and organized by Projekt DEAL.

Competing interests

The authors declare no competing interests.

Additional information

Supplementary information The online version contains supplementary material available at <https://doi.org/10.1038/s43246-021-00143-0>.

Correspondence and requests for materials should be addressed to M.K. or M.W.

Peer review information Primary handling editor: John Plummer.

Reprints and permission information is available at <http://www.nature.com/reprints>

Publisher’s note Springer Nature remains neutral with regard to jurisdictional claims in published maps and institutional affiliations.



Open Access This article is licensed under a Creative Commons Attribution 4.0 International License, which permits use, sharing, adaptation, distribution and reproduction in any medium or format, as long as you give appropriate credit to the original author(s) and the source, provide a link to the Creative Commons license, and indicate if changes were made. The images or other third party material in this article are included in the article’s Creative Commons license, unless indicated otherwise in a credit line to the material. If material is not included in the article’s Creative Commons license and your intended use is not permitted by statutory regulation or exceeds the permitted use, you will need to obtain permission directly from the copyright holder. To view a copy of this license, visit <http://creativecommons.org/licenses/by/4.0/>.

© The Author(s) 2021